Generating Bright Emissive States by Modulating the Bandgap of Monolayer Tungsten Diselenide

Tumpa Sadhukhan, and George C. Schatz*

Department of Chemistry, Northwestern University, Evanston IL 60208-3113 USA

ABSTRACT:

Transition metal dichalcogenides (TMDs) are essential due to their fascinating electronic and optical properties, strong exciton binding energy, and layer-dependent bandgap. They can be tuned to function as a single-photon emitter, but the quantum yield of photoluminescence of single-layer WSe_2 is low. There is some evidence that a bright emissive state can be produced by introducing local defects through functionalization. In this paper we use spin-polarized periodic density functional theory (DFT) to study the effect of functionalization for the specific case of cyclic carbenes. We find that the simplest of these molecules, cyclopentadiene carbene (Cyc), binds to the surface by a covalent bond leading to a substantial change in the bandgap (1.24 eV compared to 1.64 eV for the pristine surface). Moreover, there are semi-flat bands below the Fermi level that originate from σ bonding and the interaction between the lone-pair *p* orbitals on the carbon of Cyc that bonds with Se on the TMD. Cyc is found to form a Type IIa heterojunction before and after contact with the surface, where the "a" refers to ordering of the energy levels where the TMD levels have the larger splitting and "b" to the reverse. The effect of various electron-withdrawing and electron-donating groups on Cyc is investigated, and it is found that the direct bandgap and heterointerfaces can be chemically tuned with covalently bound functional groups. With an electron-withdrawing group (EWG) such as -CHO, -COCl, and -CN attached to Cyc, a Type III // Type IIa interface is formed, whereas all other EWGs used in this study form a Type IIa junction, before and after contact to the surface. The electron-donating groups (EDG) form Type Ib // Type Ia junctions, and in particular, we find that the system WSe_2 + Cyc-Me band structure consists of semi-flat bands at valence band maxima localized on Cyc-Me and the conduction band minima is coupled between the surface and functional group with a direct bandgap of 0.88 eV. Hence, we predict that the Cyc-Me functionalized monolayer WSe_2 will produce a red-shifted bright emissive state. We also find that carbenes with the Cyc all-carbon ring have (1) a triplet ground state and

(2) form covalent bonds to WSe_2, while heterocyclic carbenes (1) have a singlet ground state, and (2) do not form covalent bonds to WSe_2.

KEYWORDS: tungsten diselenide, monolayer, functionalization, cyclic carbenes, heterointerface, band structure

1. INTRODUCTION

Two-dimensional (2D) transition metal dichalcogenides (TMDs) have diverse mechanical,[1-2] electronic,[3-4] and optical properties,[5-6] making these materials versatile with an abundance of tunable features.[7-8] TMDs are widely used in catalysis,[9-10] with applications that include CO_2 reduction,[11-12] hydrogen evolution,[13-14] and water treatment,[15-16] and they are also used in photovoltaics,[17-18] energy storage,[19] quantum information.[20] In particular, TMDs exhibit strong light-matter interaction, leading to important linear and nonlinear optical properties, as well as large exciton binding energies, and spin-valley coupling.[17] Tungsten is the heaviest metal within the common family of 2D TMDs, and the larger atomic radius of W makes these 2D TMDs more flexible for the development of devices with tunable properties. However, the literature present on W-based TMDs is not extensive compared to that for Mo-based TMDs.[21] Thus, there is great interest in designing W-based TMDs and improving understanding of the electronic structure and chemical properties to obtain insights into the formation of 2D materials of technological interest. In 2005, quantum light emission in 2D semiconductors was first demonstrated in monolayer (ML) WSe_2 at low temperatures.[22-26] The scalability, robustness, and ease of handling of solid-state quantum emitters make them potentially useful in quantum computing and sensing.[27-29] One direction for this work involves the use of TMDs as single-photon emitters (SPE). SPE on WSe_2 flakes has been demonstrated using several methods which introduce defects or stains to tune electronic structure, including the bandgap.[30-32] The mechanism of SPE is not well understood in these results but it is hypothesized that the excitons are trapped by localized strain gradients or defects in the TMD flakes.[33] Defects can also be introduced by surface functionalization, producing heterojunctions, as has been done for WSe_2 with NO_2[34] and adenine.[35] These studies are related to earlier work concerning the brightening of carbon nanotube photoluminescence (PL) through the sp^3 defects introduced by covalent functionalization and the formation of type I

heterojunctions, including as described by our group[36] and others.[37] In this work, we will use density functional theory (DFT) to examine the possibilities for using functionalization of WSe_2 to generate bright emissive states which may show SPE behavior.

TMDs are composed of transition metals (TM) and chalcogens with the chemical formula MX_2, where M is TM and X is chalcogen; the TM plane is sandwiched between the X planes. Coordination of the X atom around the M atom within the monolayer (ML) can have different symmetries, such as octahedral (1T), distorted octahedral (1T'), or trigonal prismatic (2H).[38] In the ML form, the phonon dispersion of the ML trigonal prismatic (1H)[39-40] polymorph exhibits no unstable frequencies, whereas the 1T polymorph show imaginary frequencies in the range of 100i to 200i cm^{-1}.[41] Moreover, the bandgap of the TMDs also depends on the number of layers. Generally, the bulk and double layer exhibit an indirect bandgap, whereas the ML shows a direct bandgap.[42-43] Owing to these structural and electronic aspects, we selected the 1H polymorph of ML for our study.

Pristine WSe_2 has a low quantum yield for PL. In order to generate a bright emissive state, we introduce defects on the surface by functionalization. The functional groups which form a type I or Straddling gap are of interest since this helps to bypass the low-lying dark states of the pristine WSe_2. Moreover, carbenes are used as functional groups because they form systems with net spin-zero, which also helps avoid the low-energy dark states usually produced by open-shell systems. In the present study, we first consider unfunctionalized single-layer WSe_2, examining its band structure and the effect of spin-orbit coupling using several levels of DFT. Next, we characterize functionalized surfaces for three different carbenes, using the calculations to gain insight into the mechanism of chemisorption and physisorption. The nature of the band structure and energy level alignment at the carbene/WSe_2 ML junction is investigated with spin-polarized DFT, and we study how the electron-donating or -withdrawing nature of a range of functional groups attached to cyclopentadiene carbene covalently bound to the surface can modulate the bandgap, band structure, and heterojunction. Based on these studies we identify classes of covalently bound carbenes that should lead to the desired Type I band alignment.

2. METHODS

All the calculations of pristine ML WSe_2 surface and the functionalized surfaces are performed using the Vienna ab initio simulation package (VASP) based on spin-polarized density functional theory (DFT) with a plane-wave basis set and the projector-augmented wave (PAW)[44] technique. For geometry optimizations, the generalized gradient approximation (GGA) refined by Perdew, Burke, and Ernzerhof (PBE)[45] is utilized with Grimme's DFT-D3 correction;[46] and the energy- and force-convergence the parameters are 1×10^{-6} eV/cell and 1×10^{-2} eV/Å, respectively. The energy cutoff is 520 eV, and the Brillouin Zone is sampled using the Γ-centered Monkhorst−Pack k-grid scheme with a 4×4×1 supercell. Pristine WSe_2 surface is also optimized using HSE06 hybrid functional to calibrate. The Γ point (1×1×1) is employed for isolated molecules. The adsorption energy of the functional group on the surface is defined as

$$E_{ads} = E_{total} - (E_{surface} + E_{functional\_group}) \quad (1)$$

where E_{total}, $E_{surface,}$ and $E_{functional\_group}$ denote the system's total energy, the surface energy, and the isolated functional group energy, respectively. Negative adsorption energy represents an exothermic reaction. Charge transfer between the surface and the functional group is obtained from a Bader charge analysis. A negative charge difference (Δρ) indicates charge accumulation on the adsorbate, whereas a positive value refers to charge depletion. Electron localization function (ELF)[47-48] maps were evaluated to obtain information on the bonding type and electron localization. To carry out a periodic natural bond orbital (NBO) analysis, we have used a 2×2×1 supercell. The plane wave function was projected to a def2-TZVP basis set for C, H, N, S, and Se atoms, and the jorge-DZP basis set was used for W. We also did an NBO analysis for a finite model employing the 2×2×1 supercell but without periodic boundary conditions using NBO7[49] coupled with QChem[50] and B3LYP/def2-TZVP level of theory.

To understand the electronic structures, band structure calculations with and without spin-orbit coupling (SOC) were performed along the high symmetry points in the Brillouin zone (BZ) with GGA-PBE-D3, denoted as PBE-D3 and PBE-D3/SOC, respectively for pristine WSe_2 ML. We have also used the range-separated hybrid functional HSE06[51] coupled with SOC (HSE06/SOC) on the PBE-D3 geometry to evaluate the band structure and energy level alignment.

Band structures and other post-processing are carried out using VASPKIT.[52] The surface coverage calculation were calculated using Chemcraft program.[53]

3. RESULTS AND DISCUSSION

First, we study pristine WSe_2 monolayer (ML) properties at different levels of theory, followed by functionalization of the surface by carbenes. The properties of pristine WSe_2 have been studied both theoretically and experimentally in the literature,[42] so our study of pristine WSe_2 is only to calibrate our work. We have optimized the unfunctionalized pristine WSe_2 surface geometry using the HSE06 method. The W-Se bond obtained using HSE06 is 2.53Å, whereas it is 2.55Å with PBE-D3. Hence it did not lead to much structural parameter changes, as expected. Hence, we used PBE-D3 to evaluate the structural parameters for the systems under study. We selected Cyclopentadiene carbene (Cyc) as the refenced carbene for this study, and Imidazol-2-ylidene carbene (Iyc), and Thiazol-2-ylidene carbene (Tyc) as heterocyclic carbenes (**Figure 1**) for comparison. The bandgap is calculated as the difference in the energy between the highest valence K-point to the lowest conduction K′-point for the K → K′ transition.

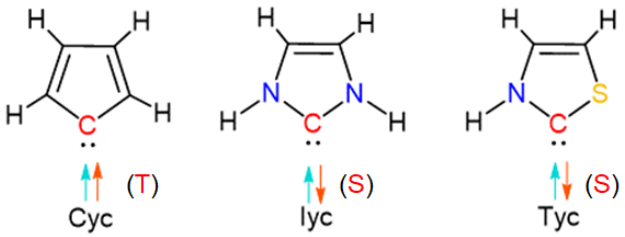

Figure 1. The structures of carbenes. T represents triplet and S singlet for the ground electronic state.

3.1 Band Structure of pristine WSe_2 Monolayer

The 4 × 4 unit cell of pristine 1H-WSe_2 ML and the band structures from PBE-D3 without and with SOC and with HSE06 with SOC (denoted HSE/SOC) are presented in **Figure S1**. This shows that ML WSe_2 has a direct bandgap of 1.64 eV based on HSE06/SOC for the K→ K′ transition. An experimental bandgap of 1.60-1.66 eV is reported in the literature.[54-58] The band character (direct bandgap) remains unchanged when calculated using the GGA functional PBE, including Grimme's dispersion interaction, D3. However, the bandgap is larger compared to

HSE06/SOC (1.50 eV with PBE-D3 and 1.21 with PBE-D3/SOC vs. 1.64 eV with HSE06/SOC), as expected since GGA functionals are known to underestimate bandgaps. The reported bandgap using PBE/SOC is 1.25 eV.[59] A splitting of 0.48 eV in the valence band maximum (VBM) and 0.04 eV in the conduction band minimum (CBM) is obtained from HSE06/SOC. The reported experimental splitting in the VBM is 0.45-0.50 eV[60], and the splitting in CBM is 0.038 eV.[61] These numbers change only slightly between simulations using the HSE06 and the PBE-D3 functional. In ML TMDs, inversion symmetry is absent, which breaks the spin degeneracy of the valence and conduction bands. The partial charge densities (**Figure S2**) indicate that the splitting originates from W. All the TMDs show similar behavior, but the magnitudes of the splitting are different. Since W is the heaviest TM in all TMDs, high-spin-orbit interaction results in the most prominent splitting among the TMDs.[62] Since HSE06/SOC performs best, we choose this level of theory for all other systems under study.

3.2 Surface Functionalization by Carbenes

The carbene functionalized ML WSe_2 surfaces are represented as WSe_2+Y, with Y being the carbene. The optimized structures of WSe_2+Cyc, WSe_2+Iyc, and WSe_2+Tyc and their lowest energy adsorption sites are shown in **Figure 2**. The adsorption sites are the H site (on top of a hexagon), TS (on top of a Se atom), and B site (on top of a Se-W-Se).

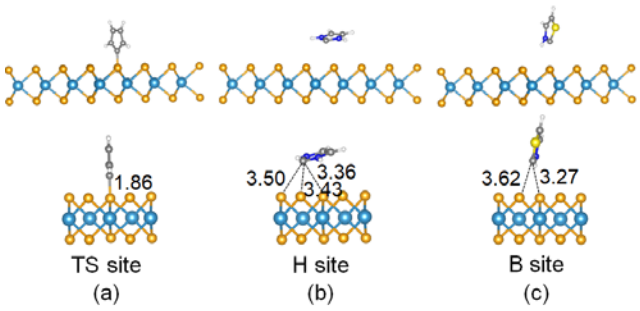

Figure 2. Side view of optimized structures of (a) WSe_2+Cyc, (b) WSe_2+Iyc, and (c) WSe_2+Tyc and their adsorption sites are represented.

The PBE-D3 results show that although the isolated Cyc carbene has a triplet ground state with a singlet-triplet energy gap ($\Delta E_{S\text{-}T}$) of 0.33 eV (**Table 1**), it binds to the WSe_2 monolayer at a TS site in a singlet state, forming a covalent bond (chemisorption), with the C−Se bond length

being 1.86 Å (**Figure 2**). The selenide atom at the TS site (Se*) is attached to 3 W atoms and the C atom (C*) of Cyc.

To understand the bonding properties, we have carried out periodic and finite molecule NBO analyses. The NBO analysis, which provides insight into lone pair (LP) orbitals as well as σ bonding and antibonding orbitals, is carried out as implemented in VASP for the periodic version and QChem for the finite molecule. Here we find that the Se* atom of the pristine WSe_2 has a LP and three σ bonding and antibonding orbitals with the three neighboring W atoms. In WSe_2+Cyc, the LP of WSe_2 participates in the σ bond formation with Cyc. The orbital occupancies in the σ orbitals decrease and σ* orbitals increase for W-Se in WSe_2+Cyc compared to the pristine ML (**Figure S3**).

From the finite molecule NBO analysis, a more detailed picture is obtained. The Wiberg bond indices of Se* in the Natural Atomic Orbital (NAO) basis are 1.5652(W), 1.5591(W), 1.5677(W), and 1.2651 (C*). Hence, Se* has a bond order > 1 with W and C*, indicating bonding beyond sigma contributions. When the isolated triplet Cyc with two unpaired electrons is adsorbed to the surface, the C* carbon is predominantly sp hybridized (2s (27.44%) and $2p_y$ (72.41%)). One of the unpaired electrons in the sp hybridized orbital of C* forms a covalent bond by sharing an electron with a predominantly spd (4s (18.56%), $5p_y$ (34.16), and $3d_{xy}$ (45.36%)) hybridized orbital of Se*. The donor-acceptor sigma bonding/antibonding (BD→BD*) interaction energy is 70.49 kcal/mol; BD occupancy being 1.76959, and BD* is 0.09988. The donor LP orbital of Se* with occupancy 1.93877 is predominantly pd hybridized ($4p_z$ (68.99%) and $3d_{yz}$ (27.16%)). The other unpaired electron of C* resides on a $2p_z$ orbital with occupancy 1.11078 forming the acceptor LP orbital. The donor-acceptor interaction energy between these orbitals, LP→LP, is 14.96 kcal/mol. These interactions are represented in **Figure 3**. These interactions in the complex explain the presence of two bands below the Fermi energy in the band structure of WSe_2+Cyc, as discussed in a later section.

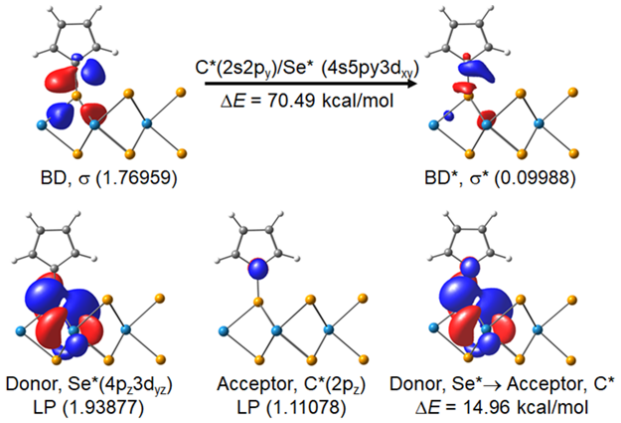

Figure 3. Finite molecule NBO analysis of WSe_2+Cyc. The orbital occupancies are indicated in parenthesis. An isovalue of 0.15 is used. ΔE represents the donor-acceptor interaction energy.

Isolated Iyc and Tyc carbenes have a singlet ground state, and they bind to WSe_2 by van der Waals interaction or charge-transfer doping with the WSe_2 monolayer (i.e., physisorption). Iyc binds to the H site, the C−Se distance being ~3.4 – 3.5 Å and the C−W distance being ~4.8 – 4.9 Å (**Figure 2**). Tyc adsorption site is to the B site, the C−Se distance being 3.3 Å and 3.6 Å (**Figure 2**). The adsorption energies for the three carbenes are **–**1.65 eV (Cyc), **–**0.52 eV (Iyc), and **–**0.39 eV (Tyc) (**Table 1**); so only the Cyc will give a stable structure under ambient conditions. The DFT calculations indicate that the paired electrons on C* are in an orbital that is 2s2p hybridized predominantly (LP orbital) both in isolated Iyc and Tyc and in WSe_2+Iyc and WSe_2+Tyc. We have also performed an ELF analysis, and we find that the electron localization and the bonding pattern obtained from the ELF map provide the same picture (as represented in **Figure S4**).

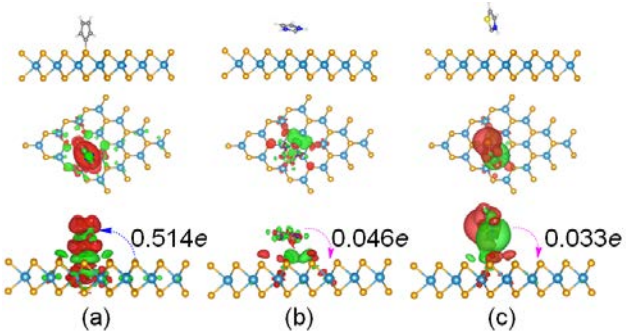

Figure 4. Charge density difference plots for (a) WSe_2+Cyc, (b) WSe_2+Iyc and (c) WSe_2+Tyc. The red (green) distribution corresponds to charge accumulation (depletion). The isosurface is taken as 5×10^{-4} e/Bohr^3. The direction and value of the Bader charge differences are also denoted.

Next, a Bader charge analysis is performed to predict the charge transfer direction and value. It is found that the Cyc carbene is a charge acceptor with 0.514e obtained from ML WSe_2, whereas Iyc and Tyc behave as charge donors, providing 0.046e and 0.033e to the ML, respectively (**Figure 4**). Although the amount of charge transfer is very small in WSe_2+Iyc and WSe_2+Tyc, the estimates of charge transfer corroborate with the weak interaction between Tyc and WSe_2, and the slightly stronger WSe_2+Iyc interaction, consistent with the adsorption energies. For Cyc adsorption on ML WSe_2, charge is transferred to the Cyc molecule, inducing a p-doping effect on the WSe_2, whereas Iyc and Tyc induce n-type doping. The magnitude of charge transfer is also many folds higher in Cyc due to chemical bond formation.

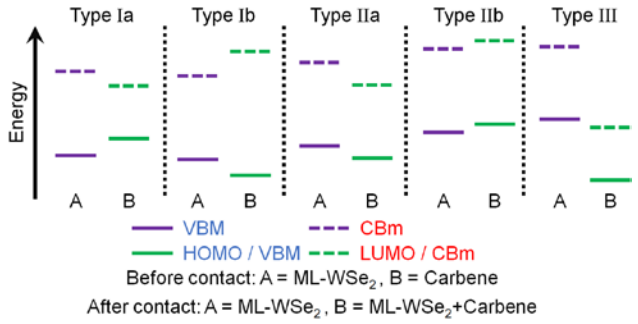

Scheme 1. Scheme of the different types of heterointerfaces formed.

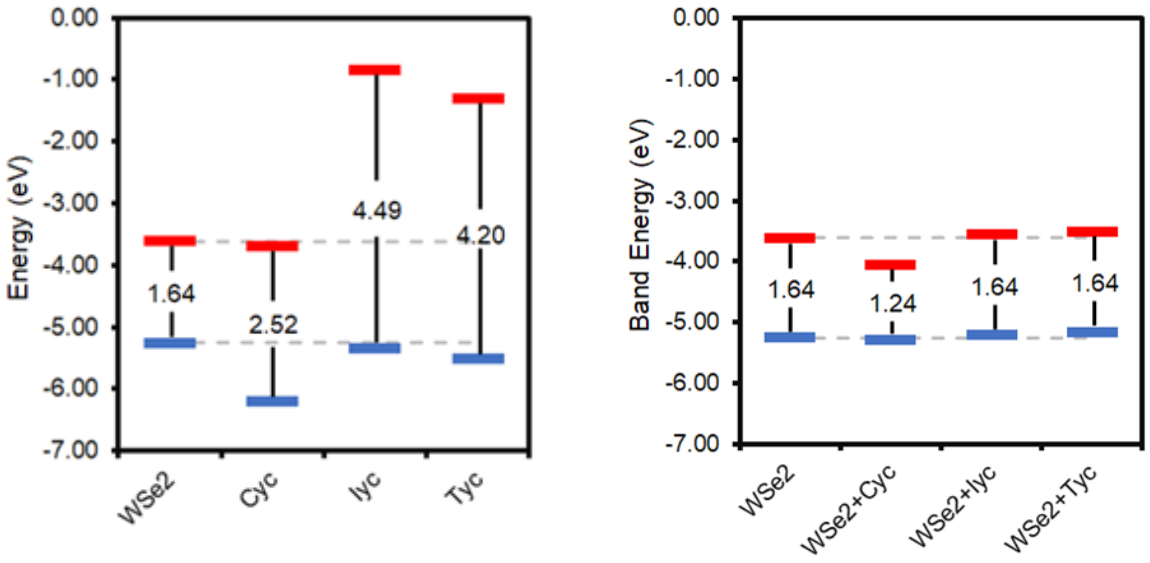

(a) (b)

Figure 5. Energy level alignment (ELA) of the (a) VBM and CBm of ML WSe_2 and the HOMO and LUMO of isolated carbene (b) VBM and CBm of WSe_2 and WSe_2+carbene. The vacuum level is set to 0 eV.

We next focus on the energy-level alignment, which can be derived from the corresponding IE and EA values.[63] **Scheme 1** represents the different types of heterointerfaces discussed in this work. Note that we distinguish between Type I junctions in which the TMD energies have a larger separation than the adsorbate (Type Ia) from the case where the TMD energies are smaller than the adsorbate (Type Ib). A similar terminology is introduced for Type II. The valence band maxima (VBM) and conduction band minima (CBm) of the pristine ML and the HOMO and LUMO of the carbene are plotted in **Figure 5(a)**, while **Figure 5(b)** shows the VBM and CBm of ML WSe_2 and WSe_2+Carbene. The band structures of the carbene functionalized surfaces are plotted in **Figure 6**.

While the isolated WSe_2+Carbene band structure provides important insight concerning electronic structure, the results in **Figures 5 and 6** are non-trivial; for example, semi-flat bands near the Fermi level are present for WSe_2+Cyc but not in WSe_2+Iyc and WSe_2+Tyc. In the complex (WSe_2+Cyc), the covalent bond between C* of Cyc and Se* of the surface and the interaction between the electron in the *p* orbital of C* in Cyc, and lone pair of Se* produces the two semi-flat bands (**Figure 6(a)**). As shown in **Figure 5(a)**, the energy band alignment of single-layer WSe_2 and the molecular energy levels of Cyc predict that WSe_2+Cyc will form type IIa heterojunction, which is consistent in ML-WSe_2/ML-WSe_2+Cyc (**Figure 5(b)**). However, **Figure 5(a)** indicates that for the separated WSe_2+Cyc species, and thus the VBM and CBm originate from WSe_2 and Cyc, respectively. These results are altered significantly when WSe_2 and Cyc interact. We see in **Figure 5(b)** that covalent interaction between the Cyc and WSe_2 reduces the LUMO level of the Cyc by 380 meV (E_{LUMO} (Cyc) – E_{CBm}(WSe2+Cyc)) and VBM of WSe_2 by 40 meV (E_{VBM} (WSe_2) – E_{VBM}(WSe2+Cyc)) in WSe_2+Cyc. **Figure 6** provides a different picture for the band structure, where the WSe_2+Cyc system has almost semi-flat occupied bands in the vicinity of the Fermi-level, indicating that these localized states originate from the Cyc molecule. The minimum energy difference between the occupied semi-flat band and CBm is found to be 1.24 eV. **Figure 7** depicts that the partial charge density of the highest occupied band lies on the Cyc molecules, whereas the lowest unoccupied bands are from W. Thus WSe_2+Cyc forms type IIa band alignment where the VBM and CBm originate from the localized Cyc and WSe_2, respectively.

Similar observations were found for 1,6-hexanedithiol functionalization of MoS_2,[64] and for MoS_2 functionalized by Cyc.[65].

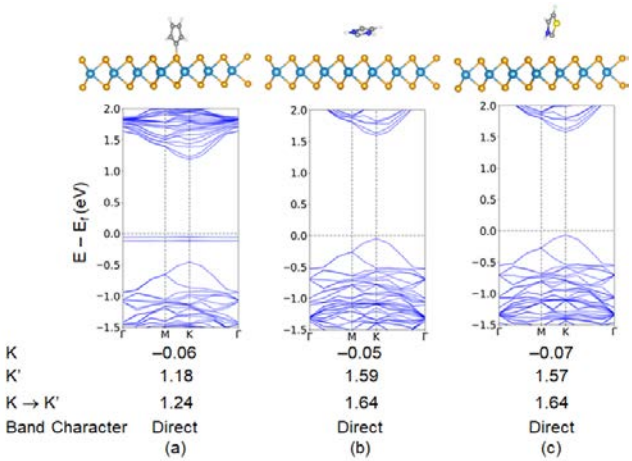

Figure 6. Optimized unit cell geometries and band structures of (a) WSe_2+Cyc, (b) WSe_2+Iyc and (c) WSe_2+Tyc.

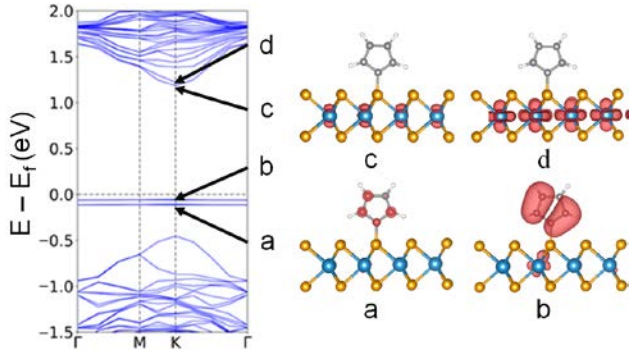

Figure 7. Electronic band structure of WSe_2+Cyc and partial charge densities at the edges of the two highest and two lowest valence and conduction bands, respectively. An isovalue of 0.0005 is used.

Now we focus on the two heterocyclic carbenes Iyc and Tyc, respectively. **Figures 5(a)** and **5(b)** reveal that the energy band edges of single-layer WSe_2 and the molecular energy levels of Iyc and Tyc are aligned to form type Ib junctions, with Iyc and Tyc having the larger gap, and in WSe_2+Iyc and WSe_2+Tyc the VBM and CBm at the junction originates from W (**Figure S5**). For the latter junctions, the VBM and the CBm move in the same direction by about 50 meV in WSe_2+Iyc and 90 meV in WSe_2+Tyc, forming type IIb junctions, and there is no change in the corresponding Kohn−Sham gap for the pristine surface (1.64 eV, K → K'). The band structures of

both WSe_2+Iyc and WSe_2+Tyc reveal the same picture, and the valence occupied bands, and unoccupied bands are not altered compared to pristine WSe_2.

Table 1. Important parameters of pristine WSe_2, isolated carbenes and functionalized surface carbenes.

	C*−Se* bond length (Å)	E_{abs} (eV)	$\|\Delta\rho\|$ e/Bohr^3	Band gap (eV)	$\Delta E_{ST} = E_S - E_T$ of isolated carbene (eV)[a]
WSe_2	-	-	-	1.64	-
WSe_2+Cyc	1.861	–1.65	0.514	1.24	0.33
WSe_2+Iyc	-	–0.52	0.046	1.64	-
WSe_2+Tyc	-	–0.39	0.033	1.64	-
WSe_2+Cyc-x, x=EWG					
WSe_2+Cyc-CHO	1.889	–1.92	0.635	1.55	0.11
WSe_2+Cyc-COMe	1.881	–1.87	0.645	1.48	0.14
WSe_2+Cyc-COOMe	1.877	–1.92	0.586	1.51	0.22
WSe_2+Cyc-COOH	1.878	–1.94	0.662	1.55	0.22
WSe_2+Cyc-COCl	1.884	–2.01	0.739	1.58	0.24
WSe_2+Cyc-CF_3	1.875	–1.97	0.684	1.57	0.24
WSe_2+Cyc-CN	1.881	–1.77	0.661	1.56	0.39
WSe_2+Cyc-x, x=EDG					
WSe_2+Cyc-OMe	1.876	–1.22	0.535	0.64	0.16
WSe_2+Cyc-OH	1.880	–0.96	0.535	0.64	0.09
WSe_2+Cyc-Me	1.939	–0.71	0.453	0.88	0.53

[a]The excited triplet electronic state calculation for the isolated Iyc and Tyc carbenes converged to singlet ground state.

Based on the results just presented, we are primarily interested in the Cyc carbene because it is adsorbed to the surface by chemisorption, which therefore shows a more substantial effect on the bandgap. Also, modulation of the bandgap is expected to be systematic when we consider substituted Cycs. In the light of these observations, we further study the substitution effect of electron-withdrawing group (EWG) and electron-donating group (EDW) on binding of the Cyc carbenes to the surface.

3.3 Effect of substitution on the Cyc carbene

In this section, we focus on the effect of substitution on the Cyc carbene by an electron-withdrawing group (EWG) at the *meta*-position and by an electron-donating group (EDG) at the *ortho*-position with respect to the C* atom of Cyc (**Figure S6**).[66] The substituted Cyc's are denoted as Cyc-x. All the isolated Cyc-x have a triplet ground state (**Table 1**). The binding nature of the Cyc-x remains the same as unsubstituted Cyc with the WSe_2 surface, i.e., chemisorption takes place at the TS site. The C−Se bond length for the Cyc-x's and the adsorption energies are presented in **Table 1**.

Many factors contribute to the variation in absorption energies of these molecules, like the deactivating (by EWG) or activating (by EDG) strength of the group x, steric effect, etc., and these in turn affect the C–Se bond length. The effect of EWGs is weaker because the substituent is attached to the *meta*-position, whereas the EDGs have a larger effect since they are attached to the *ortho*-position. The deactivating nature of the x follows the order -CHO < -COMe < -COOMe < -COOH < -COCl < -CF_3 < -CN and the order of the activating group is -OMe > -OH > -Me. For EWGs, the C-Se bond length is ~1.88-1.89 Å. In EDG, the C-Se bond length is ~1.88 Å for x = -OMe and x = -OH but increases for x = -Me to 1.94 Å, probably due to the steric effect of -Me to the surface atoms. For the the EWGs, the E_{abs} vary from ~ -1.9 to ~ -2.0 eV; Cyc-CN is -1.77 eV. A better correlation is found for x = EDG and E_{abs}. With the decrease in electron-donating strength the absorption energies decrease (E_{abs} = -1.22 eV (x = -OMe) > E_{abs} = -0.96 eV (x = -OH) > E_{abs} = -0.71 eV (x = -Me)). Irrespective of x being a EWG or EDG, the Bader charge analysis shows that all the Cyc-x pulls electron density from the surface. The order of charge withdrawal ($|\Delta\rho|$) is Cyc-Me (0.453), Cyc (0.514) < Cyc-OMe (0.535) ≤ Cyc-OH (0.535) < Cyc-COOMe (0.586) < Cyc-CHO (0.635) < Cyc-COMe (0.645) < Cyc-CN (0.661) < Cyc-COOH (0.662) < Cyc-CF_3 (0.684) < Cyc-COCl (0.739).

Now we focus on the band structure of the surface after Cyc-x functionalization (**Figure S7**) and also the energy level alignment (ELA) before and after complex formation (WSe_2+Cyc-x) (**Figure S8-S9**). For all the EWG (x=EWG), the energy level alignment of VBM and CBm of the WSe_2 surface and the HOMO and LUMO energies of the isolated carbene molecules (Cyc-x) are shown in **Figure S8.** This reveals that a type IIa heterojunction is formed except for Cyc-CHO,

Cyc-COCl, and Cyc-CN where type III junctions are predicted. Also it seems from the energy levels that the VBM would originate from the WSe_2 surface and the CBm from Cyc-x after contact and formation of type IIa junctions (**Figure S9**) as was found for WSe_2 and Cyc. Interface dipoles are formed due to charge transfer which shifts the levels at the interface.[67] For Cyc-CHO, Cyc-COCl and Cyc-CN, electron transfer from the VBM of WSe_2 to the LUMO of Cyc-x (x = -CHO, -COCl and -CN) results in positive charge on the WSe_2 and negative charge on the Cyc-x. The positive charge drives the local electrostatic potential at WSe_2 down, thus resulting in a downward shift of the levels in WSe_2. Similarly, the negative charge on Cyc-x results in an upward shift of the levels in Cyc-x. This results in a type IIa ELA at the interface (**Figure S9**).

Covalent bond formation between the surface and Cyc-x in WSe_2+Cyc-x alters the band dispersion properties at the interface. The band structures of these complexes show the presence of semi-flat occupied bands in the vicinity of the Fermi-level, indicating that these localized states originate from the Cyc-x molecule and the unoccupied CBm resembles that of the pristine surface. The splitting in the flat VBMs (**Figure S7**) originates from coupling between the Cyc-x and surface as depicted by the partial charge density plots (**Figure S10**). The bandgap in these systems ranges from 1.5 to 1.6 eV, similar to pristine ML (1.64 eV).

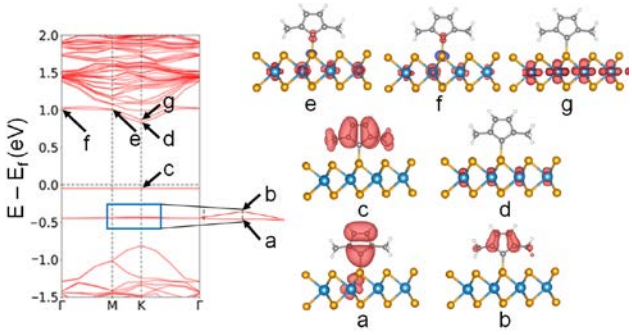

Figure 8. Electronic band structure of WSe_2+Cyc-Me and partial charge densities at the edges of the three highest and two lowest valence and conduction bands, respectively. An isovalue of 0.0005 is used.

Table 2. Types of heterojunctions formed before and after contact of the carbene with ML WSe_2.

Carbene	ML-WSe_2/Carbene // ML-WSe_2/ ML-WSe_2+Carbene
Cyc	Type IIa // Type IIa
Iyc	Type Ib // Type IIb
Tyc	Type Ib // Type IIb
x = EWG	
Cyc-CHO	Type III // Type IIa
Cyc-COMe	Type IIa // Type IIa
Cyc-COOMe	Type IIa // Type IIa
Cyc-COOH	Type IIa // Type IIa
Cyc-COCl	Type III // Type IIa
Cyc-CF_3	Type IIa // Type IIa
Cyc-CN	Type III // Type IIa
x = EDG	
Cyc-OMe	Type Ib // Type Ia
Cyc-OH	Type Ib // Type Ia
Cyc-Me	Type Ib // Type Ia

When x = EDG (-OMe, -OH, and -CH_3), in the initial state, i.e., before contact, the surface and Cyc-x valence energy levels are aligned to form a type Ib junction with Cyc-x having a wider gap component than WSe_2 (**Figure S8**). **Figure S9** predicts type Ia interface formation so that both VBM and CBm after contacts originate from the surface. In particular, the deviation between VBM and CBm for WSe_2+Cyc-Me and pristine WSe_2 is 390 meV and 370 meV, respectively, with a bandgap of 0.88 eV. However, like the WSe_2+Cyc-x (x = EWG), the band structure also shows semi-flat bands below the Fermi level, and the CBm is flat near the Γ and M k-points, which is more prominent in WSe_2+Cyc-Me than WSe_2+Cyc-OMe or WSe_2+Cyc-OH. The partial charge densities (**Figure 8**) of WSe_2+Cyc-Me show that the VBM originates from Cyc-Me and the CBm (at K) arises from W. The CBm at Γ and M shows some coupling between the molecule and surface, resulting in the semi-flat band. This observation is also supported by the projected density of states (**Figure S11**). In **Table 2** we summarize the type of heterointerfaces formed before and after contact of WSe_2 and carbenes studied in this work. We have also checked the effect on band structure on decreasing the surface area using WSe_2 4×8×1 supercell and Cpc-CH_3. We observe that the bandgap has increased for the 4×8×1 superlattice as expected, but the valence and conduction band structure remain almost the same (**Figure S12**). The surface coverage of Cpc-

CH_3 on WSe_2 4×4×1 super-cell (19.40 %, **Figure S13**) is almost twice that of Cpc-CH_3 on WSe_2 4×8×1 super-cell (10.48 %, **Figure S14**). Because Cyc-Me functionalization produces well-defined direct type Ia gaps after contact, the low-lying dark states of the pristine WSe_2 can be avoided as the system relaxes after initial excitation above the band gap. This indicates that the functionalized surfaces will produce a red-shifted bright emissive state.

4. CONCLUSION

Engineering the bandgap of materials like TMDs can improve their quantum yield as a single-photon emitter. The bandgap engineering can be carried out by various methods like alloying, applying strain, or functionalization of the surface. In this work, we have adopted the functionalization method to modulate the bandgap by adding carbenes. Carbenes have the advantage over spin ½ species such as phenyl as the adduct is always a singlet. The DFT calculations reveal that the Se atom of the surface has σ-framework with the nearest tungsten atoms (3 × W) and can interact with a Cyc and its variants that have a triplet ground state through two orbitals, one where the Se* participates in σ bond with one of the electrons in the *sp* hybridized orbital of C* in the Cyc, and the other involving a *p* orbital of C*. These interactions produce two semi-flat bands below the Fermi level of WSe_2+Cyc. The heterocyclic carbenes (Iyc and Tyc) have a singlet ground state and are physisorbed to the surface by charge transfer. We observe Type IIa and IIb heterointerfaces in WSe_2+Cyc and WSe_2+heterocyclic-carbene, respectively.

In search of functional groups which produce a Type I heterojunction in contact with the surface, we studied the effect of EWG and EDG on Cyc. The band structure of substituted Cyc and Cyc are similar. The EWG substituted Cyc forms Type IIa heterointerface after contact with the surface with VBM being localized on the carbene and the CBm on the W. The EDG substituted Cyc forms a Type Ia heterojunction in contact with the surface and the occupied valence band originating from the functional group, whereas the unoccupied conduction band is coupled between W and carbene, particularly for Cyc-Me.

This work demonstrates that (1) triplet carbenes can form a covalent bond with single-layer WSe_2, which substantially tunes the bandgap, and (2) electron-donating group substituted carbene forms a Type Ia heterojunction with the surface, which consists of occupied and unoccupied bands that are semi localized on the functional group. In particular, we predict that among the scanned functional groups, Cyc-Me carbene is a good candidate for producing a red-shifted bright emissive

state with single-layer WSe_2. In the future, a larger carbene-based material space, particularly with carbenes having triplet electronic ground states, can be screened by high-throughput and machine learning to expand the tungsten diselenide-based material space for the efficient single-photon emitters and interesting photoluminescence.

ASSOCIATED CONTENT

Supporting Information is available on the journal website. Figures S1-S10 include bandstructure and partial charge densities for pristine WSe2 using HSE06/SOC, and for the functionalized WSe_2+Cyc-x structures. Also included are periodic NBOs and ELF maps, structures of the isolated cyclopentadiene carbenes, energy level alignment of VBM and CBm results, projected density of states for WSe_2+Cpc-CH_3, band structures with different supercells, and surface area calculations.

AUTHOR INFORMATION

Corresponding Author

George C. Schatz − Northwestern University, Evanston, Illinois; orcid.org/0000-0001-5837-4740; Email: g-schatz@northwestern.edu

Other Author

Tumpa Sadhukhan −Northwestern University, Evanston, Illinois; orcid.org/0000-0003-1995-7286

Notes

The authors declare no competing financial interests.

ACKNOWLEDGMENT

This research was supported as part of the Center for Molecular Quantum Transduction, an Energy Frontier Research Center funded by the U.S. Department of Energy (DOE), Office of Science, Basic Energy Sciences (BES), under Award # (DE-SC0021314). This research was also supported

in part through the computational resources and staff contributions provided for the Quest high-performance computing facility at Northwestern University, which is jointly supported by the Office of the Provost, the Office for Research, and Northwestern University Information Technology.

REFERENCES

1. Cai, H.; Guo, Y.; Gao, H.; Guo, W., Tribo-Piezoelectricity in Janus Transition Metal Dichalcogenide Bilayers: A First-Principles Study. *Nano Energy* **2019**, *56*, 33-39.
2. Shi, W.; Guo, Y.; Zhang, Z.; Guo, W., Flexoelectricity in Monolayer Transition Metal Dichalcogenides. *J Phys Chem Lett* **2018**, *9*, 6841-6846.
3. Wang, Q. H.; Kalantar-Zadeh, K.; Kis, A.; Coleman, J. N.; Strano, M. S., Electronics and Optoelectronics of Two-Dimensional Transition Metal Dichalcogenides. *Nat Nanotechnol* **2012**, *7*, 699-712.
4. Jiao, Y.; Hafez, A. M.; Cao, D.; Mukhopadhyay, A.; Ma, Y.; Zhu, H., Metallic Mos2 for High Performance Energy Storage and Energy Conversion. *Small* **2018**, *14*, e1800640.
5. Molas, M. R.; Nogajewski, K.; Slobodeniuk, A. O.; Binder, J.; Bartos, M.; Potemski, M., The Optical Response of Monolayer, Few-Layer and Bulk Tungsten Disulfide. *Nanoscale* **2017**, *9*, 13128-13141.
6. Rivera, P.; Yu, H.; Seyler, K. L.; Wilson, N. P.; Yao, W.; Xu, X., Interlayer Valley Excitons in Heterobilayers of Transition Metal Dichalcogenides. *Nat Nanotechnol* **2018**, *13*, 1004-1015.
7. Yanfeng Chen, J. X., Dumitru O. Dumcenco, Zheng Liu, Kazu Suenaga, Dong Wang, Zhigang Shuai, Ying-Sheng Huang, and Liming Xie, Tunable Band Gap Photoluminescence from Atomically Thin Transition-Metal Dichalcogenide Alloys. *ACS Nano* **2013**, *7*, 4610-4616.
8. Xie, Y., et al., Enhancing Electronic and Optoelectronic Performances of Tungsten Diselenide by Plasma Treatment. *Nanoscale* **2018**, *10*, 12436-12444.
9. Choi, C. L.; Feng, J.; Li, Y.; Wu, J.; Zak, A.; Tenne, R.; Dai, H., Ws2 Nanoflakes from Nanotubes for Electrocatalysis. *Nano Research* **2013**, *6*, 921-928.
10. Li, B. L.; Setyawati, M. I.; Zou, H. L.; Dong, J. X.; Luo, H. Q.; Li, N. B.; Leong, D. T., Emerging 0d Transition-Metal Dichalcogenides for Sensors, Biomedicine, and Clean Energy. *Small* **2017**, *13*, 1700527.
11. Francis, S. A., et al., Reduction of Aqueous Co2 to 1-Propanol at Mos2 Electrodes. *Chemistry of Materials* **2018**, *30*, 4902-4908.
12. Xu, F.; Zhu, B.; Cheng, B.; Yu, J.; Xu, J., 1d/2d Tio2/Mos2 Hybrid Nanostructures for Enhanced Photocatalytic Co2 Reduction. *Advanced Optical Materials* **2018**, *6*, 1800911.
13. Li, Y.; Wang, H.; Xie, L.; Liang, Y.; Hong, G.; Dai, H., Mos2 Nanoparticles Grown on Graphene: An Advanced Catalyst for the Hydrogen Evolution Reaction. *Journal of the American Chemical Society* **2011**, *133*, 7296-7299.
14. Voiry, D.; Salehi, M.; Silva, R.; Fujita, T.; Chen, M.; Asefa, T.; Shenoy, V. B.; Eda, G.; Chhowalla, M., Conducting Mos2 Nanosheets as Catalysts for Hydrogen Evolution Reaction. *Nano Letters* **2013**, *13*, 6222-6227.
15. Dervin, S.; Dionysiou, D. D.; Pillai, S. C., 2d Nanostructures for Water Purification: Graphene and Beyond. *Nanoscale* **2016**, *8*, 15115-15131.

16. Liu, C., et al., Rapid Water Disinfection Using Vertically Aligned Mos2 Nanofilms and Visible Light. *Nature Nanotechnology* **2016**, *11*, 1098-1104.
17. Mak, K. F.; Shan, J., Photonics and Optoelectronics of 2d Semiconductor Transition Metal Dichalcogenides. *Nature Photonics* **2016**, *10*, 216-226.
18. Manzeli, S.; Ovchinnikov, D.; Pasquier, D.; Yazyev, O. V.; Kis, A., 2d Transition Metal Dichalcogenides. *Nature Reviews Materials* **2017**, *2*.
19. Li, X.; Zhi, L., Graphene Hybridization for Energy Storage Applications. *Chemical Society Reviews* **2018**, *47*, 3189-3216.
20. Liu, X.; Hersam, M. C., 2d Materials for Quantum Information Science. *Nature Reviews Materials* **2019**, *4*, 669-684.
21. Da Silva, A. C. H.; Caturello, N. A. M. S.; Besse, R.; Lima, M. P.; Da Silva, J. L. F., Edge, Size, and Shape Effects on Ws2, Wse2, and Wte2 Nanoflake Stability: Design Principles from an Ab Initio Investigation. *Physical Chemistry Chemical Physics* **2019**, *21*, 23076-23084.
22. Srivastava, A.; Sidler, M.; Allain, A. V.; Lembke, D. S.; Kis, A.; Imamoğlu, A., Optically Active Quantum Dots in Monolayer Wse2. *Nature Nanotechnology* **2015**, *10*, 491-496.
23. He, Y.-M., et al., Single Quantum Emitters in Monolayer Semiconductors. *Nature Nanotechnology* **2015**, *10*, 497-502.
24. Koperski, M.; Nogajewski, K.; Arora, A.; Cherkez, V.; Mallet, P.; Veuillen, J. Y.; Marcus, J.; Kossacki, P.; Potemski, M., Single Photon Emitters in Exfoliated Wse2 Structures. *Nature Nanotechnology* **2015**, *10*, 503-506.
25. Chakraborty, C.; Kinnischtzke, L.; Goodfellow, K. M.; Beams, R.; Vamivakas, A. N., Voltage-Controlled Quantum Light from an Atomically Thin Semiconductor. *Nature Nanotechnology* **2015**, *10*, 507-511.
26. Tonndorf, P.; Schmidt, R.; Schneider, R.; Kern, J.; Buscema, M.; Steele, G. A.; Castellanos-Gomez, A.; van der Zant, H. S. J.; Michaelis de Vasconcellos, S.; Bratschitsch, R., Single-Photon Emission from Localized Excitons in an Atomically Thin Semiconductor. *Optica* **2015**, *2*, 347-352.
27. Awschalom, D. D.; Hanson, R.; Wrachtrup, J.; Zhou, B. B., Quantum Technologies with Optically Interfaced Solid-State Spins. *Nature Photonics* **2018**, *12*, 516-527.
28. Atatüre, M.; Englund, D.; Vamivakas, N.; Lee, S.-Y.; Wrachtrup, J., Material Platforms for Spin-Based Photonic Quantum Technologies. *Nature Reviews Materials* **2018**, *3*, 38-51.
29. Gao, W. B.; Imamoglu, A.; Bernien, H.; Hanson, R., Coherent Manipulation, Measurement and Entanglement of Individual Solid-State Spins Using Optical Fields. *Nature Photonics* **2015**, *9*, 363-373.
30. Palacios-Berraquero, C.; Kara, D. M.; Montblanch, A. R.; Barbone, M.; Latawiec, P.; Yoon, D.; Ott, A. K.; Loncar, M.; Ferrari, A. C.; Atature, M., Large-Scale Quantum-Emitter Arrays in Atomically Thin Semiconductors. *Nat Commun* **2017**, *8*, 15093.
31. Rosenberger, M. R.; Dass, C. K.; Chuang, H. J.; Sivaram, S. V.; McCreary, K. M.; Hendrickson, J. R.; Jonker, B. T., Quantum Calligraphy: Writing Single-Photon Emitters in a Two-Dimensional Materials Platform. *ACS Nano* **2019**, *13*, 904-912.
32. Peng, L.; Chan, H.; Choo, P.; Odom, T. W.; Sankaranarayanan, S.; Ma, X., Creation of Single-Photon Emitters in Wse2 Monolayers Using Nanometer-Sized Gold Tips. *Nano Lett* **2020**, *20*, 5866-5872.
33. Chakraborty, C.; Vamivakas, N.; Englund, D., Advances in Quantum Light Emission from 2d Materials. *Nanophotonics* **2019**, *8*, 2017-2032.
34. Zhao, P., et al., Air Stable P-Doping of Wse2 by Covalent Functionalization. *ACS Nano* **2014**, *8*, 10808-10814.
35. Muhabie, A. A.; Ho, C. H.; Gebeyehu, B. T.; Huang, S. Y.; Chiu, C. W.; Lai, J. Y.; Lee, D. J.; Cheng, C. C., Dynamic Tungsten Diselenide Nanomaterials: Supramolecular Assembly-Induced Structural Transition over Exfoliated Two-Dimensional Nanosheets. *Chem Sci* **2018**, *9*, 5452-5460.

36. Piao, Y.; Meany, B.; Powell, L. R.; Valley, N.; Kwon, H.; Schatz, G. C.; Wang, Y., Brightening of Carbon Nanotube Photoluminescence through the Incorporation of Sp3 Defects. *Nature Chemistry* **2013**, *5*, 840-845.
37. Ma, X.; Hartmann, N. F.; Baldwin, J. K. S.; Doorn, S. K.; Htoon, H., Room-Temperature Single-Photon Generation from Solitary Dopants of Carbon Nanotubes. *Nature Nanotechnology* **2015**, *10*, 671-675.
38. Yun, W. S.; Han, S. W.; Hong, S. C.; Kim, I. G.; Lee, J. D., Thickness and Strain Effects on Electronic Structures of Transition Metal Dichalcogenides: 2h-Mx2 Semiconductors (M= Mo, W; X= S, Se, Te). *Physical Review B* **2012**, *85*, 033305.
39. Xu, Y.; Li, Y.; Chen, X.; Zhang, C.; Zhang, R.; Lu, P., First-Principle Study of Hydrogenation on Monolayer Mos2. *AIP Advances* **2016**, *6*.
40. Voiry, D.; Mohite, A.; Chhowalla, M., Phase Engineering of Transition Metal Dichalcogenides. *Chem Soc Rev* **2015**, *44*, 2702-12.
41. Mak, K. F.; Lee, C.; Hone, J.; Shan, J.; Heinz, T. F., Atomically Thin Mos2: A New Direct-Gap Semiconductor. *Physical Review Letters* **2010**, *105*, 136805.
42. Yun, W. S.; Han, S. W.; Hong, S. C.; Kim, I. G.; Lee, J. D., Thickness and Strain Effects on Electronic Structures of Transition Metal Dichalcogenides: 2h-$M{X}_{2}$ Semiconductors (M $=$ Mo, W; X $=$ S, Se, Te). *Physical Review B* **2012**, *85*, 033305.
43. Song, J.-G., et al., Controllable Synthesis of Molybdenum Tungsten Disulfide Alloy for Vertically Composition-Controlled Multilayer. *Nature Communications* **2015**, *6*, 7817.
44. Kresse, G. J., D., From Ultrasoft Pseudopotentials to the Projector Augmented-Wave Method. *Phys. Rev. B: Condens. Matter Mater. Phys.* **1999**, *59*, 1758-1775.
45. Paier, J. H., R.; Marsman, M.; Kresse, G., The Perdew-Burke-Ernzerhof Exchange-Correlation Functional Applied to the G2–1 Test Set Using a Plane-Wave Basis Set. *J. Chem. Phys.* **2005**, *122*, 234102.
46. Grimme, S. A., J.; Ehrlich, S.; Krieg, H. , A Consistent and Accurate Ab Initio Parametrization of Density Functional Dispersion Correction (Dft-D) for the 94 Elements H-Pu. *J. Chem. Phys.* **2010**, *132*, 154104.
47. Becke, A. D.; Edgecombe, K. E., A Simple Measure of Electron Localization in Atomic and Molecular Systems. *The Journal of Chemical Physics* **1990**, *92*, 5397-5403.
48. Savin, A.; Nesper, R.; Wengert, S.; Fässler, T. F., Elf: The Electron Localization Function. *Angewandte Chemie International Edition* **1997**, *36*, 1808-1832.
49. E. D. Glendening, J., K. Badenhoop, A. E. Reed, J. E. Carpenter, J. A. Bohmann, C. M. Morales, P. Karafiloglou, C. R. Landis, and F. Weinhold, *Nbo 7.0.*, Theoretical Chemistry Institute, University of Wisconsin, Madison: 2018.
50. Shao, Y.; Gan, Z.; Epifanovsky, E.; Gilbert, A. T. B.; Wormit, M.; Kussmann, J.; Lange, A. W.; Behn, A.; Deng, J.; Feng, X., et al, Advances in Molecular Quantum Chemistry Contained in the Q-Chem 4 Program Package. *Molecular Physics* **2015**, *113*, 184-215.
51. Heyd, J.; Scuseria, G. E.; Ernzerhof, M., Hybrid Functionals Based on a Screened Coulomb Potential. *The Journal of Chemical Physics* **2003**, *118*, 8207-8215.
52. Wang, V.; Xu, N.; Liu, J.-C.; Tang, G.; Geng, W.-T., Vaspkit: A User-Friendly Interface Facilitating High-Throughput Computing and Analysis Using Vasp Code. *Computer Physics Communications* **2021**, *267*, 108033.
53. Zhurko, G. A. Chemcraft - Graphical Program for Visualization of Quantum Chemistry Computations. Ivanovo, Russia, 2005. . https://chemcraftprog.com.
54. Gusakova, J.; Wang, X.; Shiau, L. L.; Krivosheeva, A.; Shaposhnikov, V.; Borisenko, V.; Gusakov, V.; Tay, B. K., Electronic Properties of Bulk and Monolayer Tmds: Theoretical Study within Dft Framework (Gvj-2e Method). *physica status solidi a* **2017**, *214*, 1700218.

55. Baugher, B. W. H.; Churchill, H. O. H.; Yang, Y.; Jarillo-Herrero, P., Optoelectronic Devices Based on Electrically Tunable P–N Diodes in a Monolayer Dichalcogenide. *Nature Nanotechnology* **2014**, *9*, 262-267.
56. Tonndorf, P., et al., Photoluminescence Emission and Raman Response of Monolayer Mos2, Mose2, and Wse2. *Opt. Express* **2013**, *21*, 4908-4916.
57. Zhao, W.; Ghorannevis, Z.; Chu, L.; Toh, M.; Kloc, C.; Tan, P.-H.; Eda, G., Evolution of Electronic Structure in Atomically Thin Sheets of Ws2 and Wse2. *ACS Nano* **2013**, *7*, 791-797.
58. Gong, Y.; Ye, G.; Lei, S.; Shi, G.; He, Y.; Lin, J.; Zhang, X.; Vajtai, R.; Pantelides, S. T.; Zhou, W., et al, Synthesis of Millimeter-Scale Transition Metal Dichalcogenides Single Crystals. *Advanced Functional Materials* **2016**, *26*, 2009-2015.
59. Kang, J.; Tongay, S.; Zhou, J.; Li, J.; Wu, J., Band Offsets and Heterostructures of Two-Dimensional Semiconductors. *Applied Physics Letters* **2013**, *102*, 012111.
60. Le, D.; Barinov, A.; Preciado, E.; Isarraraz, M.; Tanabe, I.; Komesu, T.; Troha, C.; Bartels, L.; Rahman, T. S.; Dowben, P. A., Spin–Orbit Coupling in the Band Structure of Monolayer Wse2. *Journal of Physics: Condensed Matter* **2015**, *27*, 182201.
61. Kośmider, K.; González, J. W.; Fernández-Rossier, J., Large Spin Splitting in the Conduction Band of Transition Metal Dichalcogenide Monolayers. *Physical Review B* **2013**, *88*, 245436.
62. Zhu, Z. Y.; Cheng, Y. C.; Schwingenschlögl, U., Giant Spin-Orbit-Induced Spin Splitting in Two-Dimensional Transition-Metal Dichalcogenide Semiconductors. *Physical Review B* **2011**, *84*, 153402.
63. Anderson, R. L., Experiments on Ge-Gaas Heterojunctions. *Solid-State Electronics* **1962**, *5*, 341-351.
64. Gul, A.; Bacaksiz, C.; Unsal, E.; Akbali, B.; Tomak, A.; Zareie, H. M.; Sahin, H., Theoretical and Experimental Investigation of Conjugation of 1,6-Hexanedithiol on Mos2. *Materials Research Express* **2018**, *5*, 036415.
65. Jones, L. O.; Mosquera, M. A.; Ratner, M. A.; Schatz, G. C., Control of Charge Carriers and Band Structure in 2d Monolayer Molybdenum Disulfide Via Covalent Functionalization. *ACS Appl Mater Interfaces* **2020**, *12*, 4607-4615.
66. Liu, S., Where Does the Electron Go? The Nature of Ortho/Para and Meta Group Directing in Electrophilic Aromatic Substitution. *J Chem Phys* **2014**, *141*, 194109.
67. Huang, Y. L.; Zheng, Y. J.; Song, Z.; Chi, D.; Wee, A. T. S.; Quek, S. Y., The Organic–2d Transition Metal Dichalcogenide Heterointerface. *Chemical Society Reviews* **2018**, *47*, 3241-3264.

TOC